



Effect of copper chromite on ammonium perchlorate decomposition-A TGA-FTIR-MS and FE-SEM study

Shani Saha¹ · Arindrajit Chowdhury¹ · Neeraj Kumbhakarna¹

Received: 15 January 2024 / Accepted: 16 June 2024 / Published online: 3 July 2024
© Akadémiai Kiadó, Budapest, Hungary 2024

Abstract

The effect of a copper chromite (CC) catalyst on the decomposition of ammonium perchlorate (AP) was investigated using thermo gravimetric analysis (TGA) in conjunction with Fourier transform infrared (FTIR) spectroscopy and electron ionization (EI) mass spectrometry (MS) of the evolved gases. To determine the activation energy of AP samples, the Kissinger–Akahira–Sunose iso-conversional method was used, which shed more light on the effect of copper chromite on both the low-temperature decomposition (LTD) and high-temperature decomposition (HTD) stages. The FTIR and mass spectra revealed species O₂, N₂O, Cl₂, NO₂, HCl, HNO₃, H₂O, ClO, HOCl, and m/z equal to 30. Using a CC catalyst, an increment in the species mole fraction was detected in the HTD stage for all the AP samples. After the catalyst was brought closer, especially when it was embedded with AP, significant changes were observed in the LTD stage as well. MS revealed the formation of new species such as HClO₄, ClO₄, HClO₃, and ClO₃ when CC is embedded in AP. Additionally, increased ClO₂ due to CC enhances the decomposition reactions near the subsurface. C-DTA proves that the effect in LTD is more due to exothermic decomposition reactions. Consequently, this overall increase in species generation leads to greater mass loss during the LTD stage decomposition. The accelerated path of NO₂ production for the pellet of mixed ammonium perchlorate and copper chromite, as well as Copper chromite embedded AP in the LTD stage, is attributed to the presence of ClO₂ and the oxidation of CC. These findings demonstrate that the presence of CC near AP causes aging, resulting in a decrease in burn rate over time. Understanding these results will aid in building a detailed chemical kinetic mechanism (DCKM) and open new avenues for researchers to use it wisely in the real world.

Keywords Ammonium perchlorate · Copper chromite · TGA · FTIR · MS

Abbreviations

E_α	Activation energy/kJ mol ⁻¹
R	Universal gas constant/J mol ⁻¹ K ⁻¹
$T_{\alpha,i}$	Temperature/K
β_i	Ith heating rate/K min ⁻¹
A	Reacted fraction
t	Time/s

Introduction

The most popular catalyst for accelerating composite solid propellant's burn rate is copper chromite (CC). Ammonium perchlorate (AP) based composite propellant is commonly utilized in booster applications due to its commercial availability, simplicity, dependability, and high specific impulse. The chemical kinetic characteristics that correspond to the thermal decomposition of AP with Copper Chromite (CC) are therefore of interest to the propellant community. When held for prolonged periods, copper chromite (CC), which is included in AP-based propellants, may slowly decompose alongside AP even at ambient settings. A summary of the vast majority of studies on propellant ageing is given by Naseem et al. [1]. If copper chromite is used, the mechanism for ageing has been demonstrated by Perumal et al. [2]. According to Perumal et al. [2] study, the burn rate of AP reduces in the presence of CC approximately after 5 years. According to XRD and EDS analysis of this study, CC is

✉ Neeraj Kumbhakarna
neeraj_k@iitb.ac.in

Shani Saha
shanisaha10@gmail.com

¹ Department of Mechanical Engineering, IIT Bombay,
Mumbai 400076, India

oxidized in presence of AP and it is assumed that there is a slow chemical reaction under the cyclic temperature loading when both are in close proximity. This chemical reaction has been investigated in detail in this work.

The Beckstead-Derr-Price model is currently being utilized by researchers to simulate the steady state combustion of AP utilizing the semi-global mechanism [3, 4]. If catalysts are used in addition to AP, no recognised mechanism exists. Also, insufficient information exists to establish the detailed chemical kinetics mechanism (DCKM). The importance of DCKM is mentioned in Mallick et al. [5]. This study will gather sufficient information for DCKM and describe how copper chromite accelerates ageing.

According to a previous study by Mallick et al. [5], the three distinct regimes make up thermal decomposition. The decomposition products of AP in LTD and HTD regimes are a mix of different species, including NO_2 , O_2 , H_2O , NO , N_2 , N_2O , HCl , Cl_2 , ClO , ClO_2 , ClO_3 , HOCl , HClO_3 , HClO_4 etc. [6–9]. Understanding how these species will change over time if copper chromite is combined with AP, and how this will impact the LTD and HTD stages, is crucial. FTIR and MS are crucial tools that help in meeting this objective. They help in understanding the components, conditions and routes that affect overall condensed phase decomposition.

According to the results described in references [10, 11], CuCr_2O_4 has little effect on the rate of thermal decomposition of AP at low temperatures up to 270 °C. However, its effect becomes more noticeable at higher temperatures (280–340 °C). So, Patil et al. [12] focused on understanding the kinetics of the HTD stage and discovered the activation energy to describe the catalytic behavior of AP decomposition. However, as the bond-breaking process begins in the LTD stage, the effect of the catalyst on ageing can be understood by looking at the behavior at that stage. CC enhances the ageing of AP-based propellant. The hypothesis is that when copper chromite and AP are mixed, 1st stage pyrolysis will be faster. Therefore, the LTD stage of decomposition for all the samples is given more attention in our work.

Overall, the novelty of this study lies in making available the data needed to develop DCKM and to increase understanding of the circumstances and chemical processes that cause AP to slowly decompose or age in the presence of catalysts. To achieve this, investigations on AP decomposition in the presence of CC were done by thermogravimetric analysis (TGA) in an open crucible, in conjunction with Fourier transform infrared (FTIR) spectroscopy and Netzsch Äelos mass spectrometry (MS) of evolved gases. AP underwent heating at three different rates to analyze how global activation energies and pre-exponential factors vary with the reacted mass fraction. Field emission quanta 200 environmental scanning electron microscopy (FE-SEM) was used to understand the topography of the samples.

Experiments

Preparation of samples

Ammonium perchlorate (AP) of particle size 300 µm and copper chromite (CC) used in this work was supplied by HEMRL Pune. The types of samples used in the experiments are shown in Table 1.

Sample II is prepared by gently stirring a mixture of 2% CC powder and AP in a glass beaker using a spatula. To create Sample III, 50 mg of AP powder is placed in a 6-mm die set and pressed using an in-house automatic hydraulic pellet press machine, applying a load of 4 tons. Sample IV is also prepared similarly, but this time, 50 mg of AP powder and 1 mg of copper chromite powder are mixed in a beaker before being transferred to a 6-mm die set.

Sample VI was prepared according to the technique used by Marothiya et al. [13]. 200 mL of water along with a magnetic stirrer was taken in the beaker and placed in the oven. The thermocouple was adjusted such that it was submerged in the solution and the temperature was set at 80 °C. 20 g of AP was added to it and left behind till it dissolved completely. After that 2% CC is added to the solution. The solution was left behind until it thickened to a paste, at which point the magnetic stirrer was removed. After that, the sample was kept at 80 °C for 6 h, it was heated for 5 h in a different container with silica gel to absorb moisture from the AP. A mortar and pestle were used for 30 s to crush it. The sample was poured into the sieve plates, which were then placed in the Retsch Sieve Shaker. After shaking, CC-embedded AP of 150–180 µm was obtained referred to here as AP+CC_150–180. For sample V, the same methodology is applied except for adding CC in the solution. After sieving a sample of 150–180 µm size AP was obtained termed as AP_150–180. The AP_150–180 mentioned is a recrystallized form of AP, prepared following the methodology outlined by Ishita and Ramkrishna [14]. Their study demonstrated the enhanced burn rate resulting from recrystallization. Additional improvement was seen when catalysts were embedded during this process [15, 16]. However, the

Table 1 Types of samples used in the experiments

Types of samples	Name of samples
Sample I	AP Powder of 300 µm
Sample II	AP powder mechanically mixed with 30 nm CC powder (AP_CC powder)
Sample III	AP pellet
Sample IV	AP_CC pellet
Sample V	AP_150–180
Sample VI	AP+CC_150–180 (embedded powder)

potential implications of this on aging have not been thoroughly investigated, prompting our efforts to gain a deeper understanding.

TGA-FTIR-MS setup for experiment

AP samples mixed with CC weighing 2 mg were placed at the bottom of an alumina crucible of 5.70 mm height and 5.30 mm inner diameter for the TGA experiment. The crucible was placed into a Netzsch 209 F1 Libra TGA without perforated covers. In slow pyrolysis, the heating rate is typically $5\text{--}15\text{ }^{\circ}\text{C min}^{-1}$. So, the sample was heated from 28 to $460\text{ }^{\circ}\text{C}$ with heating rates 5, 10, and $15\text{ }^{\circ}\text{C min}^{-1}$. The results were almost similar for all heating rates except for the shifting of the curves. A quartz tube with a length of 2 m and an inner diameter of 200 μm kept at $300\text{ }^{\circ}\text{C}$ connects the TGA with the Netzsch Alos mass spectrometer. A Teflon capillary tube with an approximate length of 1 m and an ID of 2 mm connects the TGA with the Bruker Vertex 80 FTIR spectrometer. Through these interconnected tubes, the condensed phase species were transported into the FTIR and MS diagnostic systems using a purge flow of 99.99 percent pure nitrogen at the rate of 140 mL min^{-1} . The species were ionized in the MS using an ionizing energy of 70 eV. The FTIR

spectra were acquired with a spectral resolution of 4 cm^{-1} over the $3750\text{--}600\text{ cm}^{-1}$ wavenumber range.

Results and discussion

TGA and c-DTA analysis

It is clear from Figs. 1 and 2 that, in the case of pellets, the LTD and HTD stages of AP breakdown behave differently when copper chromite is present. However, in the case of powder, only the HTD is seen to alter. When copper chromite catalyst is utilized, thermal arrest events are seen to be nearly non-existent in both scenarios. Therefore, the catalyst's impact on the various stages of AP breakdown will depend on how closely it is connected. Hence, samples V and VI come into the picture to bring CC much closer to AP according to the embedding technique. According to Professor Ramakrishna's research, the proximity of the catalyst influences how quickly AP burns [16]. In Fig. 3, instead of sample I or sample III, sample V is considered for comparison with sample VI (AP + CC_150-180) due to two reasons. First, the comparison must be done with particles of the same size, and second, when embedding CC with AP, AP is recrystallized. Therefore, the same technique should be used

Fig. 1 TGA of AP powder and AP_CC powder in an open crucible at $15\text{ }^{\circ}\text{C min}^{-1}$ heating rate

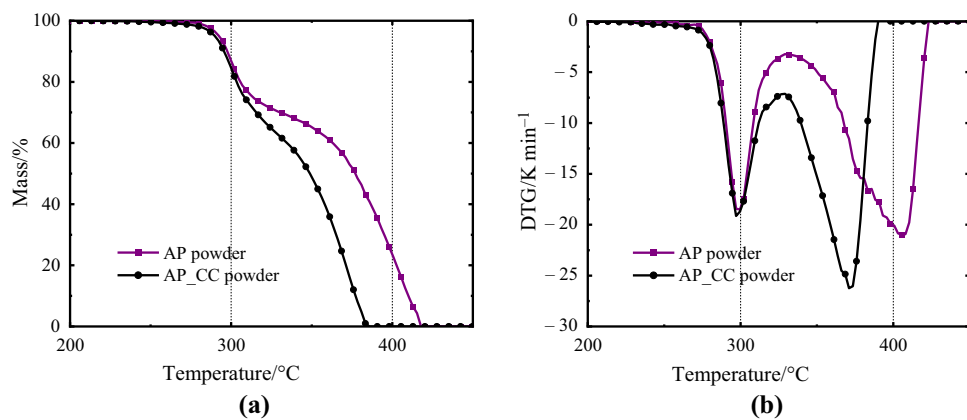


Fig. 2 TGA of AP pellet and AP_CC pellet in an open crucible at $15\text{ }^{\circ}\text{C min}^{-1}$ heating rate

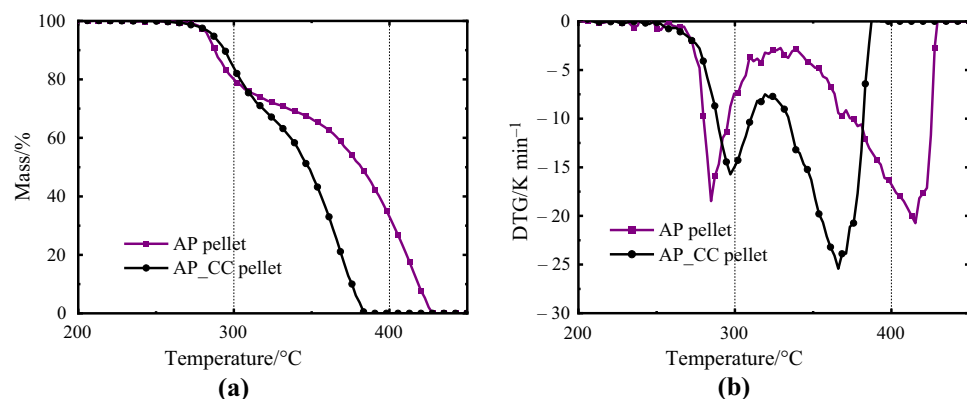
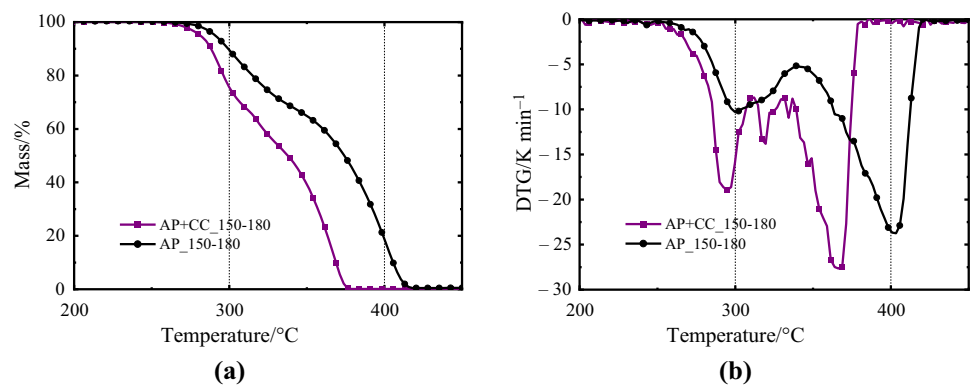


Fig. 3 TGA of AP_150-180 and AP+CC_150-180 in an open crucible at $15\text{ }^{\circ}\text{C min}^{-1}$ heating rate



without CC to prepare the sample to ensure similar sizes and morphology of AP are used for comparison. The results make it much clearer that the effect of CC is much greater in the case of the embedding technique. The sections that follow describe the most likely causes of this. These results are verified for 5, 10, and $15\text{ }^{\circ}\text{C min}^{-1}$, but pictorially only the results for the $15\text{ }^{\circ}\text{C min}^{-1}$ heating rate are shown.

c-DTA calibration is done as explained in the TGA analysis section of the reference [17] and c-DTA is used for future experiments to determine the specific process (e.g., phase change, decomposition, sublimation, and so on). Differential scanning calorimetry (DSC) analysis of AP powder and AP_CC powder is also carried out to double-check the c-DTA results. The DSC data is given in "Introduction" section of the supplementary information.

Figure 4a shows a plot of c-DTA (K) vs. Temperature ($^{\circ}\text{C}$) of AP powder and AP_CC powder in an open crucible (OC) at a heating rate of $15\text{ }^{\circ}\text{C min}^{-1}$. The first endothermic peak is related to the phase change of AP from orthorhombic to cubic [18], the second peak is the LTD stage which is exothermic and the third peak is the HTD stage which shows a shift in endothermic to exothermic behavior when CC is added. Figure 4b shows a plot of c-DTA (K) vs. Temperature ($^{\circ}\text{C}$) of AP_150-180 and AP+CC_150-180 in an open crucible (OC) at a heating rate of $15\text{ }^{\circ}\text{C min}^{-1}$. This 4(b) graph shows that the LTD stage becomes more exothermic when CC is embedded

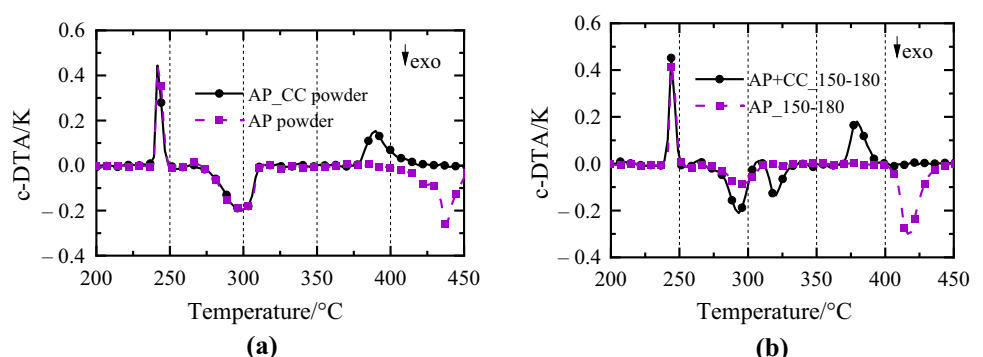
with AP, suggesting more decomposition reactions in the LTD stage. The sections that follow describe the changes in behavior in detail.

The primary cause of AP mass loss involves a combination of decomposition reactions and sublimation. During the LTD stage, decomposition reactions dominate initially starting at the nuclei, while sublimation becomes more prevalent as the reaction progresses and the surface area of AP increases, as outlined in the reference [5, 19–23]. As discussed in references [5, 19–21], the LTD stage is exothermic due to decomposition reactions and the HTD stage is endothermic due to sublimation of porous and undecomposed AP. When CC is added to AP, the exothermicity increases during the HTD stages for the powder sample, and both the LTD and HTD stages for the pellet sample. This indicates an enhancement of the decomposition reaction compared to sublimation.

Kinetic analysis

The model-free iso-conversional Kissinger–Akahira–Sunose [24] approach was used to calculate the activation energies corresponding to the various regimes of decomposition. This approach is easier and yet accurate enough to find activation energy [25]. Equation (1) defines the amount of conversion (α) samples as a function of time.

Fig. 4 **a** c-DTA (K) vs. Temperature ($^{\circ}\text{C}$) plot of AP powder and AP_CC powder in an open crucible (OC) at a heating rate of $15\text{ }^{\circ}\text{C min}^{-1}$. **b** c-DTA (K) versus Temperature ($^{\circ}\text{C}$) plot of AP_150-180 and AP+CC_150-180 in an open crucible (OC) at a heating rate of $15\text{ }^{\circ}\text{C min}^{-1}$



$$\alpha(t) = \frac{m_0 - m_t}{m_0 - m_f} \quad (1)$$

where m_t denotes the sample's mass at time t . m_0 and m_f are the sample's masses at the start and the conclusion of the procedure. The Kissinger–Akahira–Sunose approach utilizes the approximate value provided by Eq. (2)

$$\ln\left(\frac{\beta_i}{T_{\alpha,i}^2}\right) = \text{const.} - \frac{E_\alpha}{RT_\alpha} \quad (2)$$

where R is the universal gas constant, E_α is the activation energy at the degree of conversion α , $T_{\alpha,i}$ is the temperature obtained at the degree of conversion α under the i th heating rate, and β_i is the i th heating rate. The variation of the global decomposition activation energies with the reacted mass fraction was extracted using temperature-dependent changes in the AP reacted mass fraction at 5, 10, and 15 °C min⁻¹ heating rates.

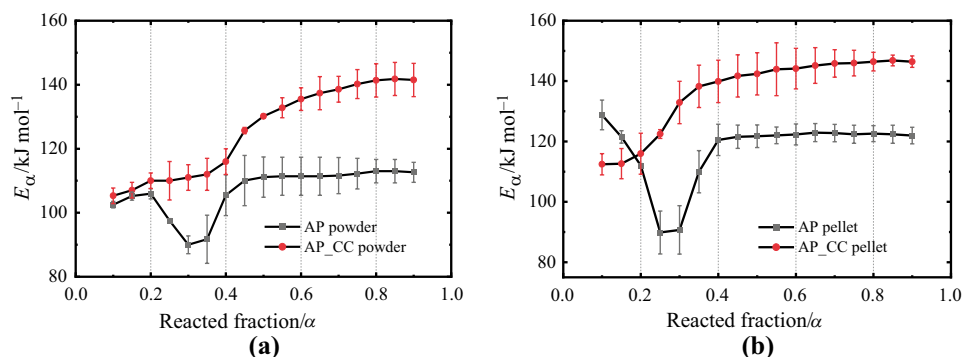
The pre-exponential factor for pellet samples is determined using the Coats–Redfern method [26] and various models mentioned in Vyazovkin et al.'s work [25], details of which are also explained in [5, 27]. The pre-exponential factor, combined with the activation energy, provides a deeper understanding of reaction kinetics [28]. The supplementary information includes the detailed procedure for determining kinetic parameters, including activation energy, pre-exponential factor, and decomposition model, for better understanding and validation of the data. In "Results and discussion" section of the supplementary information shows the accuracy of the determined kinetic parameters.

Activation energy is computed for each scenario (5, 10, and 15 °C min⁻¹), followed by averaging the obtained values and incorporating standard deviations as error bars. Figure 5a shows that the activation energy change with the reacted fraction, which is around 105 kJ mol⁻¹, is nearly identical for both AP powder and AP CC powder up to the reacted percentage of 0.2. Then, up until the fraction that has been consumed till the end of the reaction, activation energy behavior drastically changes. However, it is apparent from

Fig. 5b that the activation energy for AP pellets and AP CC pellets greatly differ not just up to the reacted fraction 0.2 but for the entirety of the reacted fraction. For the AP pellet and AP_CC pellet, the activation energy up to reacted fraction 0.2 is approximately 122 kJ mol⁻¹ and 113 kJ mol⁻¹, respectively. Therefore, the decomposition behavior of AP depends on the catalyst's closeness to it. It is noteworthy that the activation energy of AP pellets for the LTD stage is about 122 kJ mol⁻¹ as compared to 105 kJ mol⁻¹ for AP powder. According to the review by A. G. Keenan et al., the activation energy in the nuclei growth region of AP decomposition is 25 kcal mol⁻¹ and 30 kcal mol⁻¹ for AP powder and AP pellet, respectively. This has been explained by the fact that as the sample is mechanically treated, the number of crystallographic flaws decreases [29]. Since the pellet sample shows major changes, there pre-exponential factor and reaction rate values are found. The pre-exponential factor and reaction rate at room temperature of the AP pellet are 1.67×10^{10} min⁻¹ 9.53 × 10⁻¹² min⁻¹ and those of the AP_CC pellet are 2.50×10^9 min⁻¹ and 5.27×10^{-11} min⁻¹. Reference [17] explains that the reaction rate is inversely related to shelf life, implying that Copper chromite accelerates the aging process of AP.

Given our focus on aging, particular emphasis is placed on the LTD stage in the manuscript, as it marks the initiation of the bond-breaking process. However, it is interesting that a significant increase in activation energy can be observed after a reacted fraction of 0.2 when a catalyst is introduced to the AP. According to the theoretical studies of Zhu et al. [30], sublimation occurs through two pathways: direct sublimation to form NH₃ and HClO₄ gases, requiring 240 kJ mol⁻¹, or via the NH₃–H–OClO₃ complex, which then dissociates to NH₃ and HClO₄ with an energy requirement of approximately 120 kJ mol⁻¹ each. Mallick et al. [5, 31] verified these sublimation pathways by performing slow pyrolysis experiments. The increase in activation energy beyond reacted fraction of 0.2 is attributed to a change in the sublimation pathway from complex formation to direct sublimation. Hence, the first hypothesis for explaining increase in activation energy beyond reacted fraction

Fig. 5 **a** Activation energy (E_α) variation with a reacted fraction (α) for AP powder and AP_CC powder **b** Activation energy (E_α) variation with a reacted fraction (α) for AP pellet and AP_CC pellet



of 0.2 is that when CC is added to AP, some portion of the complex $\text{NH}_3\text{-H-OCLO}_3$ may transition to the gas phase along with decomposition. Whereas the remaining portion undergoes direct sublimation, resulting in a higher activation energy. The average activation energy for the AP pellet in the HTD stage is 120 kJ mol^{-1} and the pre-exponential factor (A) is $4.09 \times 10^8 \text{ min}^{-1}$. The average activation energy for the AP_CC pellet in the HTD stage is $144.4 \text{ kJ mol}^{-1}$ and the pre-exponential factor is $3.20 \times 10^{11} \text{ min}^{-1}$. Thus, the activation energy and the pre-exponential factor both increase for reacted fraction greater than 0.2 when CC is added. Therefore, the second hypothesis is, this activation energy increment could be due to the kinetic compensation effect. However, this significantly more complex HTD section, particularly with the inclusion of CC, necessitates additional investigation and computational analysis as done by Jacobs and Jones [20], as well as Zhu et al. [30].

Hence, it becomes evident that when the catalyst approaches close enough, the decomposition behavior changes due to alterations in activation energy. Consequently, the observed shift in the decomposition behavior of AP, as shown in Fig. 3, can be attributed to changes in activation energy. The next thing that requires addressing is how the proximity of the catalyst to AP influences the activation energy throughout the LTD period and what specific chemical reaction or mechanism is accountable for this effect, more details are explained in the MS analysis section.

TGA-FTIR analysis

Figure 6 shows the evolved gases' FTIR spectra at various junctions of the decomposition of the AP_CC pellet

at 15 K min^{-1} . Evolved species detected from the FTIR are HNO_3 , N_2O , HCl and NO_2 . The same species evolved from the AP sample's decomposition and were observed in the work of Mallick et al. [5]. Hence, the spectra of all the samples are not shown here. The FTIR gas cell's initial water vapor is constantly purged out by 99.9995% pure nitrogen purging. As a result, the water transmittance signal exceeds one. As a result, the rotational-vibrational bands of water vapor were removed from all of the spectra, making it impossible to accurately quantify the amount of water produced during decomposition. The Teflon capillary tube used to transfer products from TGA to FTIR has a length of 1 m, an inner diameter of 2 mm, and the purge flow rate was set at 140 mL min^{-1} . This gives an estimated residence time of 1.34 s for the gases in the tube to reach the FTIR from TGA. The estimation indicates that the gases were transferred almost instantly to the FTIR gas cell from the TGA chamber. This conclusion is based on the fact that the time needed to change the sample temperature by $1 \text{ }^\circ\text{C}$ was only 4 s, considering a heating rate of $15 \text{ }^\circ\text{C min}^{-1}$.

Each experiment's recorded spectra are post-processed to extract mole fractions of certain chemical species using an in-house code. Based on the observed spectra and the availability of line data in the HITRAN database, the chemical species data to be retrieved is selected. By making assumptions about the mole fractions of the species and using the least squares method to minimize the error, the internal algorithm creates a simulated spectrum using the line data from the HITRAN database and fits it to the experimental curve [32]. Iterations are carried out until there is a change of less than 0.01 percent in the sum of the errors between subsequent estimations. After the iterations were completed,

Fig. 6 FTIR spectra of gases evolved during AP decomposition at 15 K min^{-1} ; **a** beginning ($T=28 \text{ }^\circ\text{C}$), **b** LTD ($T=298 \text{ }^\circ\text{C}$), **c** HTD ($T=362 \text{ }^\circ\text{C}$)

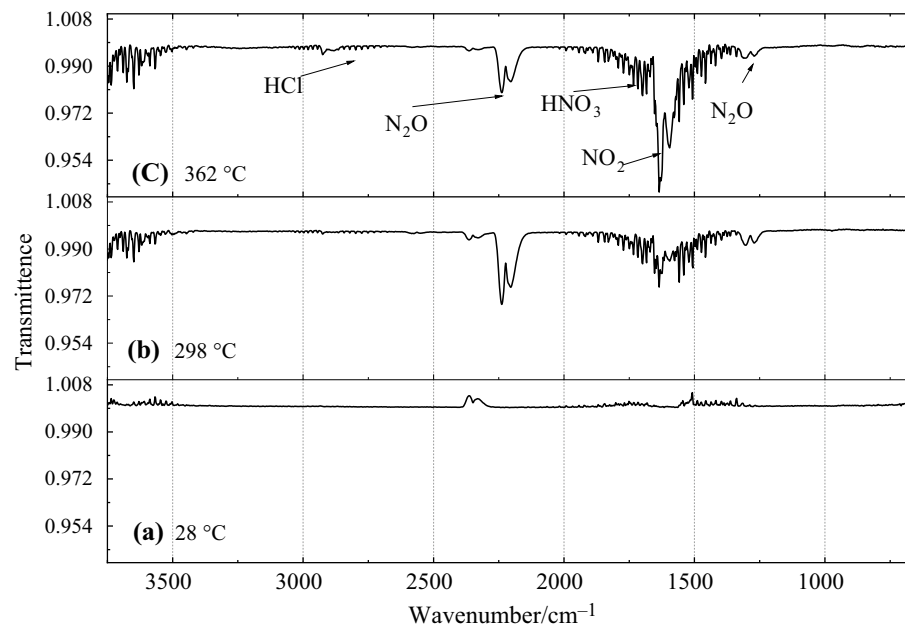


Fig. 7 **a** Variation of mole fraction (%) with Temperature ($^{\circ}\text{C}$) during AP pellet decomposition at $15\text{ }^{\circ}\text{C min}^{-1}$ on an open crucible **b** Variation of mole fraction (%) with Temperature ($^{\circ}\text{C}$) during AP_CC pellet decomposition at $15\text{ }^{\circ}\text{C min}^{-1}$ on an open crucible

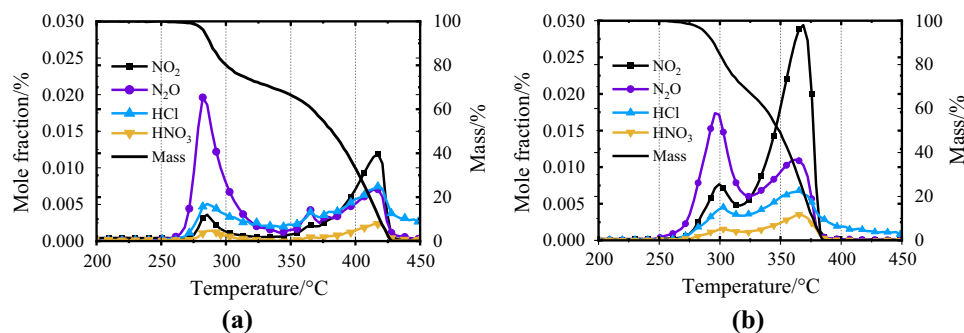
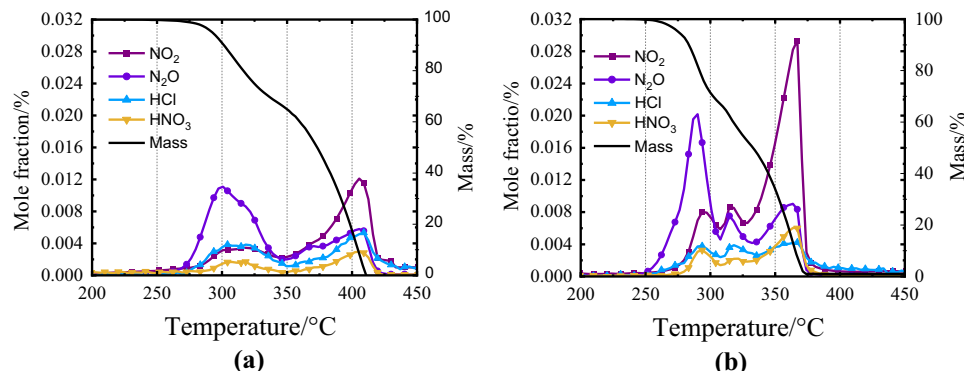


Fig. 8 **a** Variation of mole fraction (%) with Temperature ($^{\circ}\text{C}$) during AP_150-180 decomposition at $15\text{ }^{\circ}\text{C min}^{-1}$ on an open crucible **b** Variation of mole fraction (%) with Temperature ($^{\circ}\text{C}$) during AP + CC_150-180 decomposition at $15\text{ }^{\circ}\text{C min}^{-1}$ on an open crucible



the proportional mole fractions of multiple species, such as HNO_3 , N_2O , HCl , and NO_2 etc. were obtained for each spectrum.

It was discovered through the TGA analysis and kinetic analysis sections that copper chromite has an impact on the first stage if it is closely coupled with creating a compressed pellet or embedded powder. Variations in activation energy were seen in all stages for pellet samples during the AP decomposition. Therefore, to understand the causes of the different LTD stage disintegration behaviors and assist in understanding the kinetics of the processes, product profiles must be compared. The decomposition products of pellet samples are compared in Fig. 7 in this section. The relative mole fraction profiles of decomposition products of AP_150-180 and AP + CC_150-180 are compared in Fig. 8 in this section. Figure 7 shows that, like AP powder decomposition, AP pellet decomposition consists of three stages: LTD, ITD, and HTD decomposition. N_2O is dominant at the LTD stage, while NO_2 is dominant at the HTD stage. Although the behavior is similar in the case of AP_CC pellet decomposition, the mole fraction of the products in the LTD stage and HTD stage differs. Table 2 has been created to help in understanding the behavior.

Figure 7 provides insight into the concentrations of various species, yet discerning their changing ratios across different stages remains challenging. Hence, the ratios are taken to show how species concentration changes with respect to each other and what species dominates particular stages.

Table 2 Various species' mole fraction ratios obtained during the LTD stage of AP pellet and AP_CC pellet at $15\text{ }^{\circ}\text{C min}^{-1}$

Sample	$\text{N}_2\text{O}:\text{HCl}$	$\text{NO}_2:\text{HCl}$	$\text{HNO}_3:\text{HCl}$	$\text{N}_2\text{O}:\text{NO}_2$
AP pellet	3.85	0.70	0.42	5.47
AP_CC pellet	3.82	1.68	0.33	2.26

similar to the work done by Mallick et al. [5]. This also helps us to understand how catalysts change the concentration of different species. The ratio of different species' mole fractions to HCl 's mole fraction at the peak of the LTD stage is shown in Table 2. $\text{N}_2\text{O}:\text{NO}_2$ is also shown. N_2O is the dominant species for both AP pellet and AP CC pellet, and their values are quite close. However, the ratio $\text{NO}_2:\text{HCl}$ for the AP_CC pellet is rather high in comparison to the AP pellet, indicating that the copper chromite in the LTD stage also has a catalytic influence on the decomposition of the AP_CC pellet.

Table 3 also shows the ratios of mole fractions of several species with the mole fraction of HCl at the peak of the HTD stage. In the HTD stage for both pellet samples, product NO_2 prevails. The ratio for all the species is higher for the AP CC pellet compared to the AP pellet in this stage, indicating that the copper chromite catalyst's catalytic impact in the HTD stage is very dominant. After analyzing the TGA results, it became evident that copper chromite (CC) has a more significant impact on AP decomposition when embedded.

Table 3 Various species' mole fraction ratios obtained during the HTD stage of AP pellet and AP_CC pellet at $15\text{ }^{\circ}\text{C min}^{-1}$

Sample	$\text{N}_2\text{O}:\text{HCl}$	$\text{NO}_2:\text{HCl}$	$\text{HNO}_3:\text{HCl}$	$\text{N}_2\text{O}:\text{NO}_2$
AP pellet	0.95	1.60	0.32	0.59
AP_CC pellet	1.62	4.30	0.52	0.38

Table 4 Various species' mole fraction ratios obtained during the LTD stage of AP_150-180 and AP+CC_150-180 at 15 K min^{-1}

Sample	$\text{N}_2\text{O}:\text{HCl}$	$\text{NO}_2:\text{HCl}$	$\text{HNO}_3:\text{HCl}$	$\text{N}_2\text{O}:\text{NO}_2$
AP pellet	3.09	0.88	0.41	3.52
AP+CC	5.36	2.12	0.92	2.52

Table 5 Various species' mole fraction ratios obtained during the HTD stage of AP_150-180 and AP+CC_150-180 at $15\text{ }^{\circ}\text{C min}^{-1}$

Sample	$\text{N}_2\text{O}:\text{HCl}$	$\text{NO}_2:\text{HCl}$	$\text{HNO}_3:\text{HCl}$	$\text{N}_2\text{O}:\text{NO}_2$
AP pellet	1.12	2.35	0.57	2.09
AP+CC	2.15	6.98	1.44	0.31

Therefore, it is essential to compare the FTIR results of AP_150-180 and AP+CC_150-180. As depicted in Fig. 8, all species' mole fractions increase during both the LTD and HTD stages when copper chromite is present.

Furthermore, to understand the chemical reaction, a comparison of species mole fractions with the mole fraction of HCl was done and has been presented in Tables 4 and 5. Table 4 reveals that not only did all species' mole fractions increase with reference to HCl, but CC also amplified the NO_2 mole fraction increment compared to N_2O from the LTD stage itself. Moreover, Table 5 indicates that this NO_2 mole fraction becomes dominant during the HTD stage, showing an even higher mole fraction when CC is embedded. Hence, it is evident that the catalyst's effect on AP decomposition primarily involves the increment of NO_2 mole fraction compared to other species. However, the exact mechanism behind this mole fraction change remains

unclear. To shed more light on the matter, additional information about the species was gathered using mass spectrometry, which is discussed in the TGA-MS analysis section.

TGA-MS analysis

Compared to the FTIR spectra, the mass spectra showed a wider variety of species. For AP_150-180, signals of HCl, N_2O , NO_2 , Cl_2 , ClO_2 , ClO , HOCl, Cl and $m/z=30$ are found which is shown in Fig. 9a. O_2 , H_2O and NH_3 are also found for AP_150-150-180 which is not shown in Fig. 9a due to its starting range. All these species are also found for AP powder and AP pellets, which was also observed in the work of Mallick et al. [5]. Since a major change was observed in the case of AP_150-180 to AP+CC_150-180, only these sample spectra are compared. The majority of the studies have assigned the peak at $m/z=30$ to NO [6, 7], but the FTIR spectra did not allow for its definitive detection, hence NO is not used to characterize it. Because each gas also was not calibrated due to lack of calibration gas, complication and time, these MS spectra had the drawback of being unable to estimate the mole fractions of the species with certainty. However, from Fig. 9, it can be seen that using a copper chromite catalyst boosted the peak of each species in the case of AP+CC_150-180 compared to AP_150-180, suggesting that copper chromite has a significant impact on AP_CC decomposition starting from the LTD stage itself.

Figure 10a indicates no discernible peak variations for HClO_4 , ClO_4 , HClO_3 and ClO_3 even though they have higher intensity than that in Fig. 10b. Previous mass spectrometry (MS) studies conducted by Mallick et al. [5], Verneker [7], and Longuet [33] also show no evidence of these species. A recent study by Patel et al. [34] suggests that the proton transfer doesn't occur directly between NH_4^+ and ClO_4^- . Instead, ClO_4^- decomposes to yield ClO_2^- and O_2 , and the proton transfer takes place between NH_4^+ and ClO_2^- resulting in the formation of NH_3 and HClO_2 . Therefore, in both experimental and theoretical investigations, it appears that the decomposition of AP does not result in the formation of HClO_4 , ClO_4 , HClO_3 or ClO_3 .

Fig. 9 Evolved gases MS signals during decomposition of **a** AP_150-180 and **b** AP+CC_150-180 in an open crucible

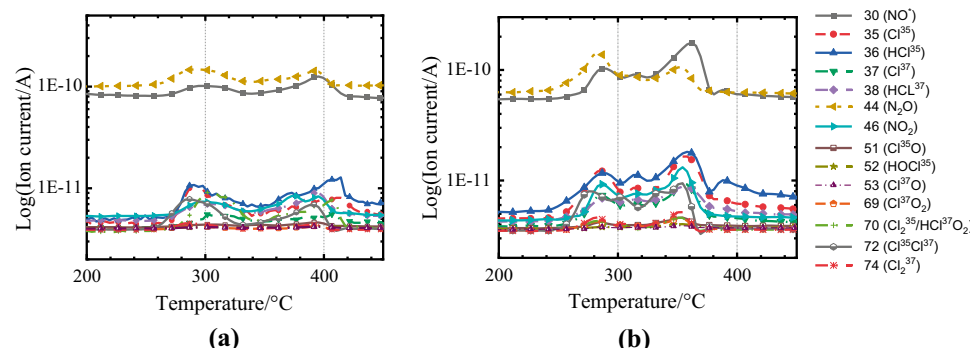
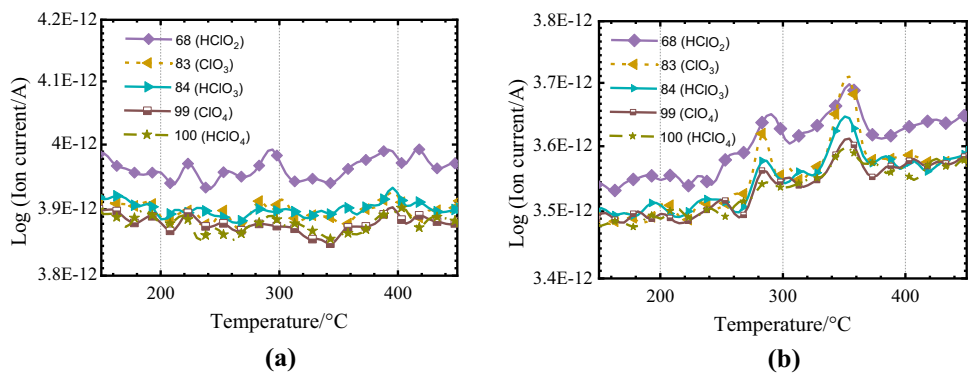


Fig. 10 Comparison between decomposition of **a** AP_150-180 and **b** AP + CC_150-180 by some MS signals of gases



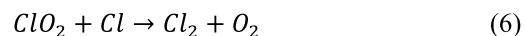
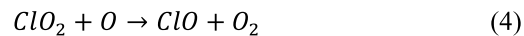
From Fig. 10b, it is evident that the embedding of CC with AP resulted in the detection of new species such as ClO_3 , HClO_3 , ClO_4 , and HClO_4 , which were not visible in any of the AP samples. This indicates that not only did the species mole fraction increase but also new species evolved due to the embedding of CC with AP. This finding is also somehow related to the increment in NO_2 species mole fraction compared to other species from the LTD stage, as discussed in the FTIR section. However, the specific reaction responsible for this phenomenon still needs to be determined. To gain a better understanding of the reactions involved, Scheme 1 has been suggested. It includes only the relevant reactions from the works of Pearson et al. [35] and Boldyrev et al. [19, 36]. It is important to note that this scheme may not be entirely accurate, and further computational studies are required to establish more reactions with

precision, which would determine the future scope of this research.

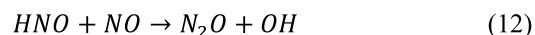
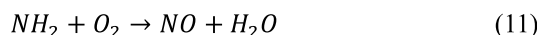
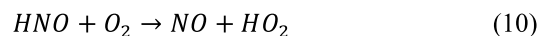
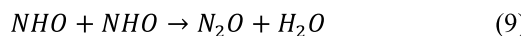
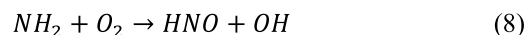
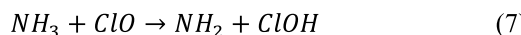
Thermal decomposition of ammonium perchlorate (AP) occurs through solid-state decomposition, sublimation, and surface reactions [20]. The first stage of AP decomposition is referred to as the Low-Temperature Decomposition (LTD) stage, which primarily involves decomposition reactions. The subsequent stage is known as High-Temperature Decomposition (HTD), primarily driven by sublimation processes [5, 21].

Raeovsky et al. [22] discussed that the LTD stage reactions initiate at dislocations in the crystal lattice located just below the crystal surface. As these dislocations grow and form nuclei, pressure develops within the nuclei, reaching approximately 20 bars. As a result, the nearby structures begin to mechanically distort, and the process continues

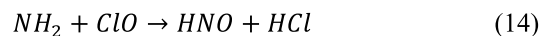
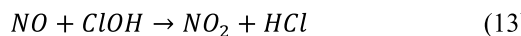
Reactions for ClO_2 , O_2 , Cl_2 and ClO formation:



Reactions for ClOH , NO^* and N_2O formation:

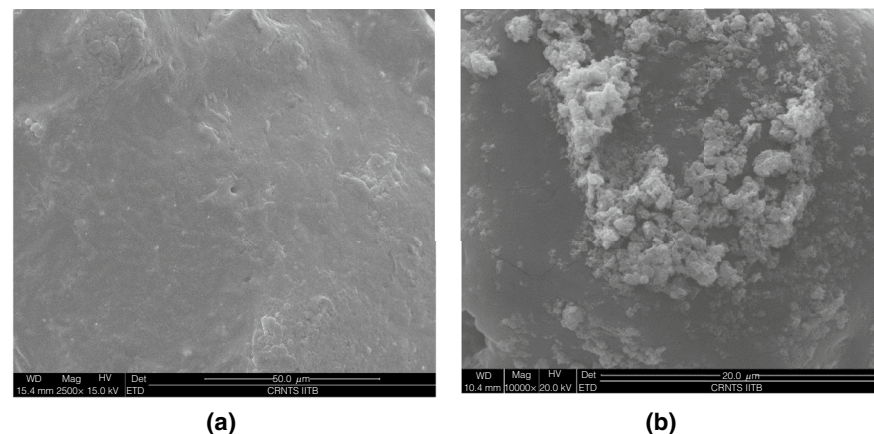


Reactions for HCl and NO_2 formation:



Scheme 1 Reaction Scheme for evolved gases from AP decomposition [35]

Fig. 11 ESEM of **a** AP_150-180 and **b** AP+CC_150-180 at room temperature



until these nuclei fill the entire structure. During the LTD regime, the gases slowly diffuse out of the nuclei and also explode out of the nuclei, resulting in the formation of a porous macrostructure [19]. This porous structure leads to an increased sublimation process in the HTD stage [5, 19]. Figure 11a displays the smooth surface of AP. When AP and CC powders are mechanically mixed, the subsurface reactions leading to the LTD stage reaction remain unchanged. However, as the products from the subsurface level reach the surface during the HTD stage, they react with CC, causing changes in the decomposition behavior regardless of the proximity of CC to AP. Nevertheless, bringing CC closer by pelletizing does show some effect, and the effect is more pronounced when CC is embedded. Figure 11b illustrates the extent of the connection between CC and the AP surface. C-DTA data also shows that the LTD stage becomes more exothermic which is due to the decomposition process of AP, when CC is embedded with AP. Therefore, when CC is embedded, it can affect the reactions near the boundaries of the nuclei, resulting in the early discharge of gases from the surface, leading to a slightly lower onset temperature and a higher rate of decomposition in the LTD stage.

To understand how embedded CC affects the subsurface level reaction, Table 6 has been compiled, where the ion current of the peak's maximum point is subtracted from the base point and presented in the table. Each ion current is proportional to the mole fraction of species but not exactly indicative of the species mole fraction. Nevertheless, this ion current data (in A) provides insights into the dominant

species when CC is embedded and how the reaction can occur.

Another noteworthy observation is the presence of HClO_4 , ClO_4 , HClO_3 , and ClO_3 in the MS signals of AP+CC_150-180. There are two possibilities for formation of HClO_4 , one is these species could result from sublimation since their formation is barrier-free, and the second is when AP and CC are in close proximity, proton transfer between ClO_4^- to NH_4^+ is possible leading to the formation of NH_3 and HClO_4 . This HClO_4 further decomposes to form a variety of chlorine oxides including ClO_2 . ClO_2 acts as the key oxidizer, catalyzing the transformation of NH_3 and NH_4^+ into various species [35, 36].

In the study by Zhu et al. [23] and Boldyrev et al. [19], it was elucidated that during the LTD stage, when the outflow of NH_3 surpasses that of ClO_2 in the local atmosphere at the subsurface site, N_2O formation exceeds that of NO_2 . As the reaction progresses, NH_3 outflow diminishes in comparison to ClO_2 , resulting in increased NO_2 formation. Therefore, if ClO_2 concentration increases NO_2 formation will also increase.

From Table 6, it is evident that the mole fraction of all species increases when CC is embedded with AP, resulting in enhanced AP decomposition in LTD. Among the species, ClO_2 and NO_2 show a more significant increase compared to others. With an increase in ClO_2 mole fraction, both O_2 and ClO production rise, as indicated by reactions 1–6 in the reaction scheme. ClO reacts with NH_3 to produce intermediate products like NO , NH_2 , and HNO as shown in the

Table 6 Peak MS signals of evolved species from AP_150-180 and AP+CC_150-180 at the peak of LTD stage decomposition

Sample	HCl	O_2	Cl	N_2O	NO_2	ClO	ClOH	ClO_2	Cl_2
AP_150-180	4.5×10^{-12}	7×10^{-11}	1.9×10^{-12}	4.4×10^{-11}	1.91×10^{-12}	2.8×10^{-13}	7×10^{-14}	2.4×10^{-13}	6.2×10^{-13}
AP+CC_150-180	6.3×10^{-12}	1.3×10^{-10}	3.22×10^{-12}	7.97×10^{-11}	4.67×10^{-12}	4.90×10^{-13}	1.3×10^{-13}	6.7×10^{-13}	1.09×10^{-12}
AP+CC_150-180: AP_150-180	1.38	1.86	1.69	1.81	2.45	1.75	1.86	2.79	1.76

reaction scheme by multiple reaction pathways. These intermediates contribute to an increase in both N_2O , NO_2 , and other species, as also observed in the FTIR results. Perumal et al. [2] observed that when AP and CC are in close proximity, CC is oxidized, producing O_2 . As the O_2 mole fraction increases significantly, reaction 17 becomes dominant compared to reaction 9, as shown by study of Pearson [35], leading to a formation of more NO_2 . As a result, we see an overall increase in species concentration with slightly more NO_2 formation.

Nevertheless, this analysis requires further investigation through computational studies similar to study of Zhu et al. [30] and Patel et al. [34] to develop a comprehensive and robust chemical kinetics mechanism for AP decomposition in the presence of a catalyst. Furthermore, the insights and data obtained from this research will serve as essential benchmarks for future endeavors in this field.

Conclusions

Using the hyphenated TGA-FTIR-MS approach, the decomposition behavior of ammonium perchlorate (AP) with copper chromite (CC) catalyst was examined under non-isothermal slow cook-off conditions. Based on the mass loss investigations, it has been observed that using AP_CC pellet or embedding CC in AP, instead of mechanically mixing CC and AP in powder form, has a significant impact on the LTD regime of AP decomposition. Copper chromite has been observed to have a similar influence on the HTD stage in all cases. Kissinger–Akahira–Sunose iso-conversional method was applied to data collected at 5, 10, and 15 °C min⁻¹ to determine the activation energies of AP powder, AP_CC powder, AP pellet, and AP_CC pellet. The activation energy of AP powder and AP_CC powder in the LTD stage is 105 kJ mol⁻¹, but 122 and 113 kJ mol⁻¹ for AP pellet and AP_CC pellet, respectively, indicating the enhanced effect of a catalyst in the LTD stage if catalysts are in close contact with AP. In the HTD stage, the effect of copper chromite is nearly identical and does not depend on its proximity to AP. The species from the AP decomposition, which comprised O_2 , Cl_2 , NO_2 , N_2O , HNO_3 , HCl , H_2O , ClO , and HOCl , were identified using the FTIR and mass spectra. Based on the MS and FTIR analyses, it was noticed that CC increases species mole fraction for all the AP samples in the HTD stage. Notably, when the catalyst was brought closer, particularly when it was embedded with AP, significant changes in mole fraction were also noted in the LTD stage. During the AP decomposition of the LTD stage, the formation of new species, such as HClO_4 , ClO_3 , HClO_3 , and ClO_3^- is observed when CC is embedded with AP. The formation of HClO_4 could be attributed to a barrier-free sublimation reaction or proton transfer between ClO_4^- to NH_4^+ . This HClO_4 further

decomposes to form a variety of chlorine oxides including ClO_2 . Furthermore, from the SEM analysis and the results of FTIR and MS, it can be understood that the presence of CC embedded with AP affects the decomposition reactions near the subsurface, resulting in the production of additional ClO_2 . C-DTA data shows that the LTD stage becomes more exothermic which is due to the decomposition process of AP, when CC is embedded with AP. The presence of ClO_2 then leads to the oxidation of NH_3 and NH_4^+ , increasing the mole fraction of other species. Consequently, this overall increase in species generation results in greater mass loss during the LTD stage. The accelerated path of NO_2 production in the pellet of mixed AP and CC, as well as CC-embedded AP in the LTD stage, can be attributed to the presence of extra ClO_2 , and O_2 from the oxidation of CC. These findings highlight that the presence of CC near AP causes slow decomposition or aging, leading to a decrease in burn rate over time. Moreover, these results will contribute to the development of a detailed chemical kinetics mechanism (DCKM), which will serve the research community in practical applications.

Supplementary Information The online version contains supplementary material available at <https://doi.org/10.1007/s10973-024-13395-y>.

Acknowledgements We would like to express our gratitude to the High Energy Materials Research Laboratory for providing samples of copper chromite and ammonium perchlorate. We are also grateful for the financial support received for this work from DRDO under grant RD/0117-COPTS00-002. Assistance from Jay Patel for helping in understanding the reactions is also greatly acknowledged.

Authors contribution Shani Saha—Designed research, performed research, analyzed data, and manuscript preparation. Arindrajit Chowdhury—Supervision and review of results. Neeraj Kumbhakarna—Supervision, review of results and manuscript editing.

References

1. Naseem H, Murthy H, Ramakrishna PA. Effect of ageing on mechanical properties of composite solid propellants. 52nd AIAA/SAE/ASEE Joint Propulsion Conference. AIAA Propulsion and Energy Forum, Salt Lake City, 2016.
2. Perumal R, Nagendra K, Ramakrishna PA. Effect of ageing on combustion of ammonium perchlorate with copper chromite additive. Combust Flame. 2020;212:352–4.
3. Beckstead MW, Derr RL, Price CF. A model of composite solid-propellant combustion based on multiple flames. AIAA J. 1970;8:2200–7.
4. Jeppson M, Beckstead M, Jing Q. A kinetic model for the premixed combustion of a fine AP/HTPB composite propellant. In 36th AIAA Aerospace Sciences Meeting and Exhibit. 1998;1–12.
5. Mallick L, Kumar S, Chowdhury A. Thermal decomposition of ammonium perchlorate—A TGA–FTIR–MS study: part I. Thermochim Acta. 2015;610:57–68.
6. Heath GA, Majer JR. Mass spectrometric study of the thermal decomposition of ammonium perchlorate. Trans Faraday Soc. 1964;60:1783–91.

7. Verneker VRP, Maycock JN. Mass spectrometric study of the thermal decomposition of ammonium perchlorate. *J Chem Phys.* 1967;47:3618–21.
8. Korobeinichev OP, Boldyrev VV, Karpenko YY, Lyakhov NZ. Investigation of rapid processes in the thermal decomposition of ammonium perchlorate with a transit time mass spectrometer. *Bull Acad Sci.* 1969;18:706–8.
9. Kokobeinichev P, Anisiforov GI, Tereschenko AG. High-temperature decomposition of ammonium perchlorate–polystyrene–catalyst mixtures. *AIAA J.* 1975;13:628–33.
10. Solymosi F. Initiation of ammonium perchlorate – ignition by chromic oxide titanium dioxide catalysts. *Combust Flame.* 1965;9:141.
11. Rosser WA, Inami SH, Wise H. Thermal decomposition of ammonium perchlorate. *Combust Flame.* 1968;12:427.
12. Patil PR, Krishnamurthy VN, Joshi SS. Effect of nano-copper oxide and copper chromite on the thermal decomposition of ammonium perchlorate. *Propell Explos Pyrotech.* 2008;33:266–70.
13. Marothiya G, Vijay C, Ishitha K, Ramakrishna PA. Effects on burn rates of pellets and propellants with catalyst-embedded AP. *J Propuls Power.* 2018;34:969–74.
14. Ishitha K, Ramakrishna PA. Development of a high burn rate non-aluminized composite propellant with low burn rate pressure index. *AIAA 2011–5559. In 47th AIAA/ASME/SAE/ASEE Joint Propulsion Conference & Exhibit;* 2011.
15. Nanda JK, Ramakrishna PA. Development of AP/HTPB based fuel rich propellant for solid propellant ramjet. *In 49th AIAA/ASME/SAE/ASEE Joint Propulsion Conference;* 2013.
16. Marothiya G, Vijay C, Ishitha K, Ramakrishna PA. An effective method to embed catalyst on AP and its effect on the burn rates of aluminized composite solid propellants. *Combust Flame.* 2017;182:114–21.
17. Saha S, Bhattacharjee A, Bhagat S, Kumar A, Pawar R, Singh S, Namboothiri INN, Chowdhury A, Kumbhakarna N. Theoretical, structural, and thermal aspects of nitro-HTPB as a prospective energetic binder—a detailed computational and experimental analysis. *Mater Today Commun.* 2024;38: 107892.
18. Kraeutle KJ. The thermal decomposition of orthorhombic ammonium perchlorate single crystals. *J Phys Chem.* 1970;74:1350–6.
19. Boldyrev VV. Thermal decomposition of ammonium perchlorate. *Thermochim Acta.* 2006;443:1–36.
20. Jacobs PW, Jones RA. Sublimation of ammonium perchlorate. *J Phys Chem.* 1968;72:202–7.
21. Lang AJ, Vyazovkin S. Effect of pressure and sample type on decomposition of ammonium perchlorate. *Combust Flame.* 2006;145:779–90.
22. Raevsky AV, Manelis GB, Boldyrev VV, Votinova LA. On the role of dislocations in thermal decomposition of ammonium perchlorate crystals. *Dokl AN SSSR.* 1965;160:1136–7.
23. Zhu YL, Huang H, Ren H, Jiao QJ. Kinetics of thermal decomposition of ammonium perchlorate by TG/DSC-MS-FTIR. *J Energ Mater.* 2014;32:16–26.
24. Akahira T, Sunose T. Joint convention of four electrical institutes, research report. 16, Chiba Institute of Technology. Science and Technology. 1971;22–31.
25. Vyazovkin S, Burnham AK, Criado JM, Pérez-Maqueda LA, Popescu C, Sbirrazzuoli N. ICTAC kinetics committee recommendations for performing kinetic computations on thermal analysis data. *Thermochim Acta.* 2011;520:1–19.
26. Coats AW, Redfern JP. Kinetic parameters from thermogravimetric data. *Nature.* 1964;201:68–9.
27. Saha S, Chowdhury A, Kumbhakarna N. Errata and comments on “Thermal decomposition of ammonium perchlorate—A TGA–FTIR–MS study: part I” [Thermochim. Acta 610 (2015) 57–68]. *Thermochim Acta.* 2024;731:179639.
28. Vyazovkin S. Determining pre-exponential factor in model-free kinetic methods: how and why? *Molecules.* 2021;26:3077.
29. Galwey K, Jacobs PWM. The thermal decomposition of ammonium perchlorate at low temperatures. *Proc R Soc Lond Ser Math Phys Sci.* 1960;254:455–69.
30. Zhu R, Lin MCJ. Mechanism and kinetics for ammonium perchlorate sublimation: a first-principles study. *J Phys Chem C.* 2008;112:14481–5.
31. Mallick L, Kumar S, Chowdhury A. Thermal decomposition of ammonium perchlorate—a TGA–FTIR–MS study: part II. *Thermochim Acta.* 2017;653:83–96.
32. Mallory CF, Thynell ST. Species and temperature profiles of propellant flames obtained from FTIR absorption spectroscopy. *Combust Sci Technol.* 1997;122:113–29.
33. Longuet B, Gillard P. Experimental investigation on the heterogeneous kinetic process of the low thermal decomposition of ammonium perchlorate particles. *Propell Explos Pyrot.* 2009;34:59–71.
34. Patel J, Panchal H, Chowdhury A, Kumbhakarna N. Initiation step in the condensed phase decomposition process of ammonium perchlorate. *ChemistrySelect.* 2023;8:1–7.
35. Jacobs PWM, Pearson GS. Mechanism of the decomposition of ammonium perchlorate. *Combust Flame.* 1969;13:419–30.
36. Gritsan VI, Panfilov VN, Boldyrev VV. Investigation of the formation of chlorine dioxide during thermal decomposition of ammonium perchlorate. *Dokl AN SSSR.* 1969;187:1082–4.

Publisher's Note Springer Nature remains neutral with regard to jurisdictional claims in published maps and institutional affiliations.

Springer Nature or its licensor (e.g. a society or other partner) holds exclusive rights to this article under a publishing agreement with the author(s) or other rightsholder(s); author self-archiving of the accepted manuscript version of this article is solely governed by the terms of such publishing agreement and applicable law.